frontiers | Frontiers in Physics

TYPE Original Research
PUBLISHED 08 December 2025
DOI 10.3389/fphy.2025.1691928

OPEN ACCESS

EDITED BY
Feng Xu,
Nanjing University of Posts and Teleco-mmunications, China

REVIEWED BY
Tan Qu,
Xi'an University of Electronic Science and Technology, China
Jing Bai,
Xi'an University of Posts and Telecommunications, China

*CORRESPONDENCE
Hamad M. Alkhoori,
hamad.alkhoori@uaeu.ac.ae

RECEIVED 24 August 2025
REVISED 22 October 2025
ACCEPTED 06 November 2025
PUBLISHED 08 December 2025

CITATION
Arfan M, Alkhoori HM, Hussein M, Althobaiti S and Althobaiti A (2025) Unraveling the electromagnetic interaction of a Bessel pincer light-sheet beam by a metamaterial PEMC sphere.
Front. Phys. 13:1691928.
doi: 10.3389/fphy.2025.1691928

Unraveling the electromagnetic interaction of a Bessel pincer light-sheet beam by a metamaterial PEMC sphere

Muhammad Arfan[1], Hamad M. Alkhoori[2]*, Mousa Hussein[2], Saad Althobaiti[3] and Ali Althobaiti[4]

[1]Department of Physics, University of Agriculture, Faisalabad, Pakistan, [2]Department of Electrical and Communication Engineering, United Arab Emirates University, Al Ain, United Arab Emirates, [3]Department of Sciences and Technology, Ranyah University College, Taif University, Taif, Saudi Arabia, [4]Department of Mathematics, College of Science, Taif University, Taif, Saudi Arabia

The interaction of a Bessel pincer light-sheet beam (BPLSB) with a metamaterial perfect electromagnetic conductor (PEMC) sphere is analyzed using the generalized Lorenz–Mie theory (GLMT). The electric field of the BPLSB is expanded by utilizing the vector angular spectrum decomposition method (VASDM). The electromagnetic fields (incident and scattered) are reconstructed by utilizing the vector spherical wave functions (VSWFs) and expanded beam shape coefficients (BSCs). Implementing the boundary conditions (BCs) on a metamaterial PEMC sphere yields the unknown expansion coefficients of the scattered electromagnetic fields. Unlike earlier GLMT studies that used plane wave or simple Bessel beams, the BPLSB source for a metamaterial PEMC sphere is employed. To investigate the electromagnetic scattering dynamics, the impacts of various configuration parameters of BPLSB, like beam order and beam scaling parameter, in addition to electromagnetic admittance and size parameter of the PEMC sphere, are analyzed meticulously. The scattering characteristics of BPLSBs by a metamaterial PEMC sphere are numerically analyzed in terms of scattering efficiency and scattering intensity in the far-field/far-zone region. This work will aid in exploring scattering and propagation, electromagnetic radiation force and torque, optical manipulation, optical tweezers, and light-matter interactions.

KEYWORDS

Bessel pincer light-sheet beam, electromagnetic scattering, generalized Lorenz-Mie theory, metamaterials, PEMC sphere

1 Introduction

Investigation of light beams through metamaterials presents significant Challenges for researchers of the optical community, mainly owing to the uncertain scattering of light [1]. Natural materials do not hold the required characteristics that are essential in electromagnetics. The distinctive features of metamaterials are caused by the interaction of electric fields and magnetic fields (electromagnetic fields) of specific order [2]. Researchers have shown significant interest in metamaterials as an evolving technology in optics, electronics, photonics, and other fields because of their remarkable characteristics for electromagnetic interaction [3].

There are several applications for electromagnetic metamaterials, including telecommunication, information and detection systems, optical manipulation, surface improvement technology, metallic antennas, and others, which pique the interest of optical researchers due to their exceptional characteristics [4]. One such renowned metamaterial is known as perfect electromagnetic conductor (PEMC) [5]. The defining feature of the PEMC is that it possesses the attributes of both a perfect electric conductor (PEC) and a perfect magnetic conductor (PMC). The light beam scattered by a PEMC metamaterial comprises both co-polarized and cross-polarized field components. Electromagnetic energy or power of any type cannot propagate through the PEMC medium [6]. It can be used as a boundary material for incident electromagnetic fields. The use of PEMC as a boundary material makes it lossless, non-reciprocal, and an isotropic, i.e., having the same physical properties in all directions. PEMC characteristics are defined by the scalar admittance parameter M. When $M = 0$ and $M \to \pm\infty$, PEMC is changed to PMC and PEC, respectively.

Furthermore, researchers have conducted comprehensive studies on the scattering of structured light beams by a PEMC [7, 8]. Due to the straightforward configuration of the metamaterial PEMC sphere, several studies have addressed the scattering characteristics of the PEMC sphere using structured light beams [9, 10]. The interaction between a structured light beam and the metamaterial PEMC sphere, characterized by a relatively tangible structure, has increasingly garnered attention. In contrast to plane waves, beams with arbitrary shapes and polarizations are more influential in scattering due to their distinct features. Consequently, an increasing number of investigations have concentrated on the interaction study between a metamaterial PEMC sphere and structured shaped beams characterized by comparatively simple forms, including Gaussian, Airy, and Hermite–Gaussian (HG) beams [8, 11, 12].

The characteristics of linearly polarized Bessel beams (LPBs) are not limited to axial Poynting flux, polarization consistency, propagation stability, exhaustive field depth, and axial-core structure [13, 14], whereas Bessel pincer light-sheet beams (BPLSBs) have characteristics such as manageable longitudinal fields, remarkable non-diffraction, improved gradients of transverse intensity, and unique signatures towards electromagnetic scattering [15, 16]. Some of the reasonable analysis between LPBs and BPLSBs is discussed in terms of polarization and longitudinal fields, energy and momentum flux, field topology, and impact of PEMC scattering [8, 17–19].

The polarization and longitudinal fields of a BPLSB are spatially organized, thus permitting control E_z, whereas LPB is marked by homogeneous linear polarization and feeble field strength E_z. This allows for synchronized transverse magnetic (TM) as well as transverse electric (TE) excitation across the PEMC boundary. LPBs carry significant axial Poynting flow, while BPLSBs boost transverse energy and reduce axial momentum. This results in lowering the radiation-pressure surroundings and makes surface interaction much better. The LPB field structure has a unique on-axis core, while the BPLSB field structure has a thin light-sheet topology with a center null. This makes the gradient of transverse intensity larger, and the real scaling parameter of BPLSB (α_0) can be used to modify the sheet thickness. The constitutive relations of the PEMC structure couples' electromagnetic fields indicate that BPLSB's higher transverse intensity gradient enhance cross-polarized components more than those of LPB.

Unraveling light-sheet beams (LSBs) may result in considerable advancements in electromagnetics and optics. So various studies, such as measurement of particle sizing [20], electromagnetic scattering [21, 22], beam shaping engineering [23], particle dynamics [24], microscopy [25], cell imaging [26], and optical manipulation [27], have been done. Many different kinds of structured beams as well as LSBs have been investigated. Several types of structured beams, including LSBs, have been examined. The scattering of a BPLSB by a charged particle has been explored using the generalized Lorenz–Mie theory (GLMT) [15]. Numerical analysis of the electromagnetic radiation force of BPLSB on a dielectric sphere has been done [28]. A comparative study of LSBs, i.e., Bessel and Bessel–Gauss, has been discussed [29]. Interaction of BPLSBs with a small sphere covered by a layer of plasmonic material has been computed [16]. Within the context of GLMT, the scattering of Bessel pincer light-sheet beams (BPLSBs) by a dielectric sphere has been analyzed [17]. The PEMC scattering characteristics irradiated by the Bessel beam have been analyzed and discussed [30, 31]. The generation of photonic nanojets from a PEMC sphere illuminated by a polarized Bessel beam was examined [32]. The diffraction-free Lommel beams for the metamaterial PEMC sphere have been investigated [33]. The scattering of diffraction-free Tricomi beams for spherical scatterer particle has been explored [34]. The radar cross section (RCS) and electromagnetic radiation force on a PEMC sphere have also been computed and discussed [35, 36].

The scattering characteristics of BPLSB in metamaterial PEMC media are currently undocumented. So, this study examines the scattering of a BPLSB by a PEMC sphere, motivated by the optical applications of BPLSB, utilizing the GLMT. The framework of GLMT is very versatile for exploring structured shaped beams using various metamaterial structures. It is an excellent technique to calculate the beam shape coefficients (BSCs) for structured light beams. This approach calculates scattering efficiency and angular distributions reliably under various situations. Additionally, this technique is efficient for linear electromagnetic scattering phenomena but may struggle with significant multi-body interactions in metamaterials. However, it has some limitations. First, GLMT may not be useful for more complex material absorption or scattering characteristics at higher frequencies, causing real-world discrepancies. The approach also requires spherical symmetry, which may limit its relevance for non-spherical objects. Furthermore, exploring the large-scale optical systems with numerous scattering sites can make GLMT computationally expensive. Additionally, increased complexity is involved for high orders or very large size parameters.

Light manipulation and light-sheet microscopy need meticulous control of electromagnetic scattering from shaped beams. Metamaterials such as those of PEMC structures provide tunable boundary conditions (BCs) that traditional materials do not show. The BPLSB's illumination of a metamaterial PEMC sphere by employing the GLMT is examined, addressing its configuration parameters—a scheme not previously explored in GLMT research. To explore the study, the following contribution involved: (i) a GLMT model tailored for PEMC with electromagnetic coupling specified by the PEMC scalar admittance parameter; (ii) computation of far-field scattering intensity and scattering efficiency

using scattering field coefficients with dimensionless size parameter and scattering angle as observable parameters for beam order, beam scaling parameter, and PEMC scalar admittance.

The layout of the work is organized as follows. The second section describes the analytical calculation of the scattering of the BPLSB by a metamaterial PEMC sphere. On the basis of analytical theory proposed in section 2, the numerical results of the far-field/far-zone scattered electric field intensity, when a BPLSB interacts with a PEMC sphere, are analyzed. Section 3 reveals the numerical results, followed by extended computational results on the influence of the electromagnetic admittance M, dimensionless size parameter of the PEMC sphere ρ, and BPLSB configuration parameters, i.e., l and α_0 which are known as order of beam and scaling parameter, on the electromagnetic scattering characteristics of the metamaterial PEMC sphere. The final section of this study presents the conclusions.

2 Theoretical formulations

The electric field of the BPLSB can be written by using the vector angular spectrum decomposition method (VASDM) of plane waves in terms of Cartesian coordinates about any $\boldsymbol{z}$ plane, such as [28, 29].

$$E_x(y,z) = \int_{-\infty}^{+\infty} S_x(p,q) e^{ik(py+qz)} dp \tag{1}$$

The angular spectrum of BPLSB, i.e., $S_x(p,q)$ can be denoted as

$$\begin{aligned} S_x(p,q) &= \left(\frac{kE_0}{2\pi}\right) \int_{-\infty}^{+\infty} J_l(\alpha_0 ky) e^{-ikpy} dy \\ &= \frac{E_0 i^{-l}}{k(\alpha_0)^l \sqrt{\alpha_0^2 - p^2}} \Re\left\{\left(p + i\sqrt{\alpha_0^2 - p^2}\right)^l\right\} \end{aligned} \tag{2}$$

α_0 is known as the beam scaling parameter regarding the BPLSB, while E_0 indicates the amplitude of the electric field. The l parameter specifies beam order. $k = \frac{2\pi}{\lambda}$ is the expression for the complete wave number phase constant. Here, (p,q) represents directional angles as $p = sin\ \alpha$ and $q = cos\ \alpha$, respectively. The angle α indicates the angle of propagation. So, with the substitution of the above-mentioned angular spectrum in Equation 1, the modified electric field of the BPLSB can be given as

$$E_x(y,z) = \left(\frac{kE_0}{2\pi}\right) \int_{-\infty}^{+\infty} \left\{ \int_{-\infty}^{+\infty} J_l(\alpha_0 ky) e^{-ikqy} dy \right\} e^{ik(py+qz)} dp \tag{3}$$

Equation 2 represents the angular spectrum, while the modified field of the BPLSB is given in Equation 3.

Consider the interaction of BPLSB with its polarized electric field in the z direction and propagation vector lying in the $xz-$ plane within BPLSB in Figure 1. The BPLSB field is influenced by the electromagnetic scalar admittance parameter of the PEMC sphere and the incident beam shape coefficients (BSCs) of the BPLSB. The PEMC sphere has a radius. The surrounding medium is considered to be air. The PEMC sphere is located in $Oxyz$ coordinate systems. The time variation factor, i.e., $e^{-i\omega t}$ is suppressed from the rest of the theoretical model for convenience.

On the basis of the GLMT [37, 38], incident and scattered electromagnetic beam fields for the BPLSB can be written as a product of unknown BSCs, i.e., (p_{mn}, q_{mn}) as expansion coefficients and vector spherical wave functions (VSWFs) as [32]

$$\boldsymbol{E}_{BPLSB}^{inc} = -\sum_{n=1}^{\infty} \sum_{m=-n}^{n} iE_{mn} \left[p_{mn} \mathbf{N}_{mn}^{(1)} + q_{mn} \mathbf{M}_{mn}^{(1)} \right] \tag{4}$$

$$\boldsymbol{E}_{BPLSB}^{sca} = \sum_{n=1}^{\infty} \sum_{m=-n}^{n} iE_{mn} \left[a_{mn}^{sca} \mathbf{N}_{mn}^{(3)} + b_{mn}^{sca} \mathbf{M}_{mn}^{(3)} \right] \tag{5}$$

$$\text{with } E_{mn} = i^n E_0 \sqrt{\frac{2n+1}{n(n+1)} \frac{(n-m)!}{(n+m)!}}$$

The vectors $\mathbf{M}_{mn}^{(1,3)}$ and $\mathbf{N}_{mn}^{(1,3)}$ denote VSWFs. The superscript 1 is used for incident fields, with the spherical Bessel functions $j_n(kr)$ involved. For scattered fields, the superscript 3 is used, and spherical Hankel functions of the first kind $h_n^1(kr)$ are included in the field expressions.

The expansion coefficients p_{mn} and q_{mn} of Equations 4, 5 can be expressed as [17]

$$p_{mn} = k \frac{i^{1-m}}{E_0} \sqrt{D}_{mn} \int_{\alpha=0}^{\pi/2} e^{-ikcos\alpha z_0} S_x(\alpha)\, \pi_n^m(cos\,\alpha)\ cos\ \alpha d\alpha \tag{6}$$

$$q_{mn} = k \frac{i^{1-m}}{E_0} \sqrt{D}_{mn} \int_{\alpha=0}^{\pi/2} e^{-ikcos\alpha z_0} S_x(\alpha)\, \tau_n^m(cos\,\alpha)\ cos\ \alpha d\alpha \tag{7}$$

Equations 6, 7 express the expansion coefficients.

Here, $D_{mn} = \frac{2n+1}{n(n+1)} \frac{(n-m)!}{(n+m)!}$. where, $\pi_n^m(.)$ and $\tau_n^m(.)$ denote angular dependent functions.

Following are the tangential and radial boundary conditions (BCs) that can be used to obtain the unknown scattering coefficients, i.e., a_{mn}^{sca} and b_{mn}^{sca} from the boundary of the PEMC spherical surface [39].

$$\boldsymbol{H}_{BPLSB}^{inc}\big|_{t(r=a)} + M\boldsymbol{E}_{BPLSB}^{inc}\big|_{t(r=a)} + \boldsymbol{H}_{BPLSB}^{sca}\big|_{t(r=a)} + M\boldsymbol{E}_{BPLSB}^{sca}\big|_{t(r=a)} = 0 \tag{8}$$

$$\epsilon_0 \boldsymbol{E}_{BPLSB}^{inc}\big|_{r(r=a)} + \epsilon_0 \boldsymbol{E}_{BPLSB}^{sca}\big|_{r(r=a)} - M\mu_0 \boldsymbol{H}_{BPLSB}^{inc}\big|_{r(r=a)} - M\mu_0 \boldsymbol{H}_{BPLSB}^{sca}\big|_{r(r=a)} = 0 \tag{9}$$

Equations 8, 9 constitute the BCs of the metamaterial PEMC sphere. Where terms t and r represent tangential and radial components, respectively. Tangential represents the electromagnetic fields that run along the surface of the PEMC sphere; it governs coupling of surface modes, while radial specifies the electromagnetic fields that point into or out of the PEMC surface; it governs how staunchly the wave interacts with the spherical surface. PEMC metamaterial performs and enforces a combination of electric and magnetic fields, i.e., electromagnetic fields, commonly known as field action at the PEMC surface. The factor M is known as the coupling parameter. It turns into PMC ($M \to 0$) and PEC ($M \to \infty$).

The incident BPLSB is written in VSWFs employing BSCs, i.e., p_{mn} and q_{mn}. The scattered field includes the unknown scattering coefficients a_{nm}^{sca} and b_{nm}^{sca}. Applying the PEMC BCs at $r = a$, besides matching the components of electromagnetic fields, it forms a system of linear equations that are solved for coefficients of scattered fields. Thus, implementation of the above-mentioned BCs, the

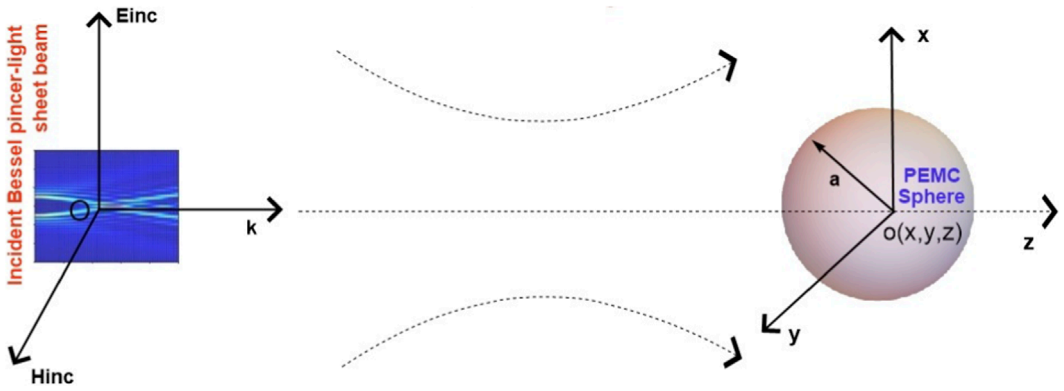

FIGURE 1
Geometry of BPLSB and metamaterial PEMC sphere for analyzing the interaction model. The intensity distribution of BPLSB with incident beam wavelength $\lambda = 0.633\,\mu m$ has been employed.

scattering field undetermined coefficients a_{nm}^{sca} and b_{nm}^{sca} can be achieved as

$$a_{nm}^{sca} = p_{mn}a_n + q_{mn}b_n \tag{10}$$

$$b_{nm}^{sca} = q_{mn}c_n + p_{mn}d_n \tag{11}$$

Equations 10, 11 establish the undetermined coefficients as a result of the application of BCs on the PEMC sphere, in which the scattering coefficients (a_n, b_n, c_n, d_n) regarding the PEMC sphere are given as [39]

$$a_n = -\left(\frac{j_n(ka)\left[ka * h_n^{(1)}(ka)\right]' + M^2\eta_0^2 h_n^{(1)}(ka)[ka * j_n(ka)]'}{(1+M^2\eta_0^2)h_n^{(1)}(ka)\left[ka * h_n^{(1)}(ka)\right]'} \right) \tag{12}$$

$$b_n = -\left(\frac{h_n^{(1)}(ka)[ka * j_n(ka)]' + M^2\eta_0^2 j_n(ka)\left[ka * h_n^{(1)}(ka)\right]'}{(1+M^2\eta_0^2)h_n^{(1)}(ka)\left[ka * h_n^{(1)}(ka)\right]'} \right) \tag{13}$$

$$c_n = M\eta_0\left(\frac{j_n(ka)\left[ka * h_n^{(1)}(ka)\right]' - h_n^{(1)}(ka)[ka * j_n(ka)]'}{(1+M^2\eta_0^2)h_n^{(1)}(ka)\left[ka * h_n^{(1)}(ka)\right]'} \right) \tag{14}$$

$$d_n = M\eta_0\left(\frac{j_n(ka)\left[ka * h_n^{(1)}(ka)\right]' - h_n^{(1)}(ka)[ka * j_n(ka)]'}{(1+M^2\eta_0^2)h_n^{(1)}(ka)\left[ka * h_n^{(1)}(ka)\right]'} \right) \tag{15}$$

Equations 12–15 constitute the scattering field coefficients of plane wave scattering by the spherical surface of the PEMC sphere.

In the traditional Mie theory, only the scattering coefficients a_n and b_n are included in the expression of the scattered fields. However, in this situation, the scattering coefficients c_n and d_n must be involved since $\boldsymbol{E}$ and $\boldsymbol{H}$ blend in the BCs. These two new coefficients show the cross-polarized parts regarding the scattered field.

when $M = 0$, PMC sphere case is attained as,

$$a_n = -\left(\frac{[ka * j_n(ka)]'}{\left[ka * h_n^{(1)}(ka)\right]'} \right); b_n = -\left(\frac{j_n(ka)}{h_n^{(1)}(ka)} \right) \tag{16}$$

For $M \to \pm\infty$, the case of the PEC sphere is achieved as,

$$a_n = -\left(\frac{j_n(ka)}{h_n^{(1)}(ka)} \right); b_n = -\left(\frac{[ka * j_n(ka)]'}{\left[ka * h_n^{(1)}(ka)\right]'} \right) \tag{17}$$

Equations 16, 17 designate the scattering coefficients for the sphere of the PMC and the PEC.

These limiting cases show that for the PMC or PEC sphere, only the co-polarized components, i.e., a_n and b_n persist, while the cross-polarized field components, i.e., c_n and d_n vanish. When the BSCs are attained, the optical efficiencies, i.e., extinction, scattering, and absorption, can also be achieved.

$$Q_{sca} = \left(\frac{2}{\rho}\right)^2 \sum_{n=1}^{\infty}\sum_{m=-n}^{n} \frac{2n+1}{n(n+1)}\left(|a_{nm}^{sca}|^2 + |b_{nm}^{sca}|^2\right) \tag{18}$$

$$Q_{ext} = \left(\frac{2}{\rho}\right)^2 \sum_{n=1}^{\infty}\sum_{m=-n}^{n} \frac{2n+1}{n(n+1)} Re(q_{mn}b_{nm}^{*sca} + p_{mn}a_{nm}^{sca}) \tag{19}$$

As extinction efficiency (Q_{ext}) can be written as the total of the scattering efficiency (Q_{sca}) and absorption efficiency (Q_{abs}) as

$$Q_{ext} = Q_{abs} + Q_{sca} \tag{20}$$

Equation 18 dictates scattering efficiency while, the Equations 19, 20 define extinction efficiency.

As no loss of energy occurs inside the PEMC sphere so $(Q_{abs} = 0)$, then by the feature of the principle of energy conservation $(Q_{ext} = Q_{sca})$. So, the ongoing numerical results of scattering efficiency for a metamaterial PEMC sphere will be computed.

The intensity of scattered light beam concerning the vertical and horizontal scattering planes are given as $I_{\perp}(\theta,\varphi) = \left(\frac{1}{k^2r^2}\right)|S_1(\theta,\varphi)|^2$ and $I_{\parallel}(\theta,\varphi) = \left(\frac{1}{k^2r^2}\right)|S_2(\theta,\varphi)|^2$ [37]. Consequently, by using the scattering field coefficients, the far-field/far-zone scattering intensity (FSI) can be expressed as

$$I^{sca}(\theta,\varphi) = I_{\perp}(\theta,\varphi) + I_{\parallel}(\theta,\varphi) \tag{21}$$

The FSI is expressed in Equation 21, where $S_1(\theta,\varphi)$ and $S_2(\theta,\varphi)$ denote amplitude functions

$$S_1(\theta,\varphi) = \sum_{n=1}^{\infty}\sum_{m=-n}^{n} E_{mn}(-i)^n\left[a_{nm}^{sca}\pi_n^{|m|}(\cos\theta) + b_{nm}^{sca}\tau_n^{|m|}(\cos\theta)\right]e^{im\varphi} \tag{22}$$

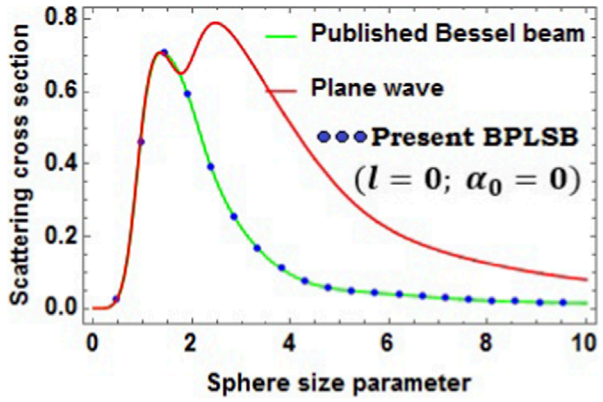

FIGURE 2
Comparison between our present work for zeroth order BPLSB ($l = 0$) and beam scaling parameter ($\alpha_0 = 0$) and plane wave scattering for metamaterial PEMC sphere. The rest of the parameters are adopted as, $\lambda = 0.633\mu m$, and PEMC admittance $M = 5$.

$$S_2(\theta,\varphi) = \sum_{n=1}^{\infty}\sum_{m=-n}^{n} E_{mn}(-i)^n\left[a_{nm}^{sca}\tau_n^{|m|}(\cos\theta) + b_{nm}^{sca}\pi_n^{|m|}(\cos\theta)\right]e^{im\varphi} \tag{23}$$

Equations 22, 23 form scattering amplitudes.

3 Numerical results and discussion

Based on the analytical calculations given in Section 2, the BPLSB with wavelength $\lambda = 0.633\mu m$ irradiating the metamaterial PEMC sphere is considered. The numerical results are focused and discussed in terms of FSI and scattering efficiency. Right here, the influence of varying the scattering angle θ on FSI is emphasized. However, for scattering efficiency (Q_{sca}), the dimensionless size parameter of the PEMC sphere, is varied as $0-15$. The impact of the scalar admittance, i.e., M of the PEMC sphere, is emphasized in addition to configuration parameters of BPLSB for far-fields. The field amplitude E_0 in all the numerical results is set as $1\,N/C$. In free space, the wave impedance η_0 is defined as unity; therefore, $M\eta_0$ is considered as a single entity and is represented as M. Regarding numerical analysis, the beam parameters are kept as $l = 1$, $\alpha_0 = 0.1$, and $M = 5$ unless mentioned otherwise.

For the validation of the numerical results, the scattering cross-section for the scattering of the BPLSB from the metamaterial PEMC sphere has been plotted. The configuration parameters regarding the BPLSB are set as the beam order $l = 0$, and the beam scaling parameter regarding the BPLSB $\alpha_0 = 0$. It demonstrates that adequate conformity is achieved, which ensures certainty of the outcomes of electromagnetic scattering of plane wave and Bessel beam by the PEMC sphere [30, 39]. Figure 2 illustrates the numerical outcomes of this comparison.

The impacts of the electromagnetic admittance parameter (M) on far-field scattered intensities for a PEMC sphere illuminated by a BPLSB are illustrated in Figure 3. Figures 3a,b correspond to the cases for which $M = 0, 2, 5$, and ∞, respectively. The case of PEMC evolves as scalar admittance M goes through $0, \pm\infty$. In these figures, the scattered intensities of the PEMC sphere first amplify and afterward suppress as M parameter increases $(0, 2, 5, \infty)$ around the scattering angle $\approx 1.5\,rad$. The trend of scattering pattern repeats in a reversing order after a scattering angle of $\approx 1.5\,rad$. The PEMC sphere's scattering comeback happens because the incident electromagnetic fields and the scattered electromagnetic fields interfere with each other. The scattering effect becomes more noticeable as M grows $(2, 5)$ because the scattered intensity distributes due to the interference phenomena for the PEMC surface. Additionally, the distribution of incident light beam intensity significantly contributes to the scattering of the PEMC sphere concerning the scalar admittance parameter M, alongside interference. Admittance is the fundamental parameter for adjusting the scattering field response of a metamaterial PEMC sphere.

The co-polarized field represents the scattered field component that is parallel to the polarization of the incident field, whereas the cross-polarized field indicates the component that is perpendicular to the polarization of the incident field. The PEMC boundary conditions (BCs) make things uneven, modifying the way both the field components, i.e., co-polarized and cross-polarized scatter, and it depends on the admittance of the PEMC sphere. The PEMC parameter yields improved control over electromagnetic scattering and propagation characteristics.

The limiting cases of PEMC are explored when it degenerates to PMC $(M = 0)$ and PEC $(M \to \pm\infty)$. The replacement of electromagnetic admittance for PMC and PEC results in the presence of only co-polarized scattered field components, with cross-polarized field components being eliminated. Considering scattering intensity for limiting cases, i.e., PMC and PEC, the scattering lobes are closer to each other. For the PEC and PMC cases, only the co-polarized scattering field components are involved, and consequently the PEC and PMC scattering curves are displayed with the same magnitude. The PEC surface completely reflects the incident electromagnetic fields. This causes substantial backscattering of co-polarized components and very little scattering of cross-polarized field components *in lieu* of normal incidence. The PMC surface captures merely the incident field's perpendicular component, affecting polarization-dependent scattering. This condition makes the cross-polarized field more noticeable in certain scattering directions.

The effects of the dimensionless size parameter, i.e., $(\rho = ka)$ on scattered intensities for a metamaterial PEMC spherical surface irradiated by BPLSB, are illustrated in Figure 4. Figures 4a,b correspond to the cases for which $\rho = 3, 4, 5$ and 6, respectively. In these figures, the scattered intensities of the PEMC sphere increase as the ρ parameter increases $(3, 4, 5, 6)$ in the E-plane. However, for the E-plane, more influence of the dimensionless size parameter of the PEMC spherical sphere for scattered intensities can be seen. This behavior arises from the scattering response of a homogeneous spherical surface of metamaterial PEMC, which is a result of the interference between the incident and scattered electromagnetic fields. Also, augmenting the dimensionless size parameter of the PEMC sphere, more of the incident BPLSB illuminates the homogeneous PEMC sphere. The scattering effect becomes more obvious as ρ augments $(3, 4, 5, 6)$ because the scattered field intensity distributes itself. Metamaterial PEMC sphere illuminated by BPLSBs exhibit improved scattered intensities since sphere of larger size

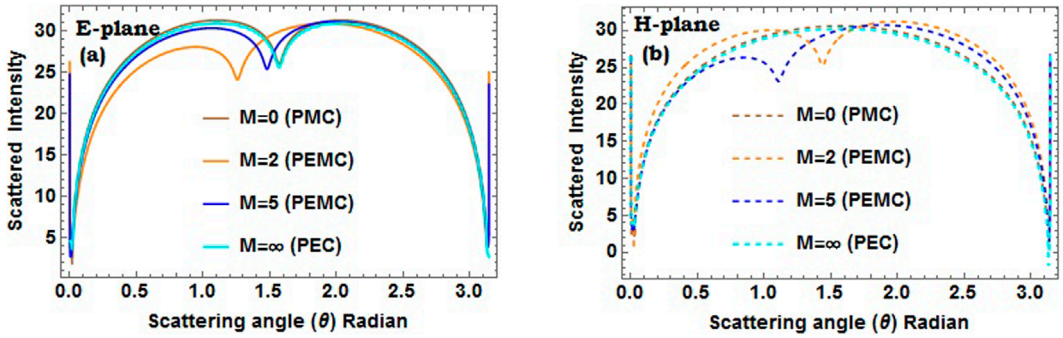

FIGURE 3
Far-field scattered intensity for PEMC sphere for various electromagnetic admittance (M) with $l = 1$, $\rho = 2$, and $\alpha_0 = 0.1$ **(a)** E-plane **(b)** H-plane.

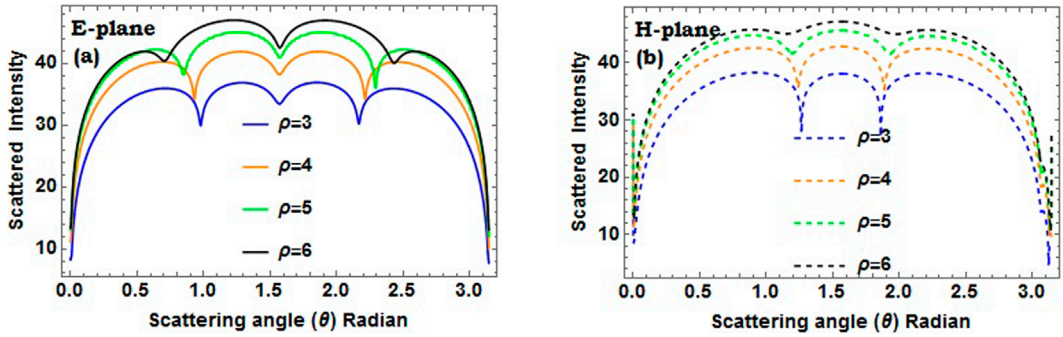

FIGURE 4
Far-field scattered intensity for PEMC sphere for various dimensionless size parameter (ρ) with $l = 1$, $\alpha_0 = 0.1$, and $M = 5$ **(a)** E-plane **(b)** H-plane.

interacts with a larger fraction of the incident BPLSB and support further resonant field modes. The far-zone scattered intensity augments as a result of improved multipole excitations and an enhanced scattering cross-section.

As the size parameter grows, the interaction between the incident BPLSB and the metamaterial PEMC sphere becomes intricate because of various scattering effects and the fact that higher-order multipoles become more significant. However, for PEMC spherical surfaces, these processes are also affected by the BCs, which influence both the co-polarized fields and the cross-polarized field components. Furthermore, as the dimensionless size augments, the co-polarized besides cross-polarized scattering field become more sensitive due to the enhanced electromagnetic interaction of the BPLSB's order with the large sphere's surface. Also, for increased size parameter, boosted interference patterns develops, which results in enhanced scattering. Thus, the PEMC surface is valuable in optics for optical manipulation and modifying the electromagnetic scattering characteristics.

Figure 5 illustrates the impact of the beam order (l) on the distribution of far-field/far-zone scattered intensity of BPLSB. The order of the beam is varied as ($l = 1, 2, \& 3$). The beam intensity related to BPLSB decreases owing to the interaction of the beam topological charge and beam order with the PEMC sphere. The basic reason for the involvement of inner field modes linked with different beam orders, such as ($l = 1, 2, \& 3$). Bessel beams of higher order have less energy in the center and more energy on the off-center side lobes. This means that less energy is focused on the metamaterial PEMC sphere, which makes it less excited and drops the intensity distribution of the scattered light beam. Due to a lower energy concentration at the beam center, less light interacts with the spherical surface of the PEMC sphere, reducing the distribution of scattered intensity. Principally, the beam gets less concentrated, leaving less energy available for electromagnetic scattering. The decrease in scattered intensity with increasing order (l) of the BPLSB is the reduction in the beam's operative focal region. Higher-order Bessel beams become less focused on a specific focal point. This results in a repressed interaction volume with the metamaterial PEMC sphere, generating less effective coupling between the BPLSB and the spherical surface. Consequently, this leads to a decrease in the energy density at the interaction location, dictating weaker optical scattering.

In Figure 6, the impact of the beam scaling parameter (α_0) on the BPLSB scattered intensity can be realized. For the metamaterial PEMC sphere, the beam scaling parameter (α_0) of a BPLSB significantly excites the field intensity distribution due to their promising role in forming the beam's focal characteristics, beam size, and intensity distribution. It can be seen that increasing the scaling parameter, such as $(0.3, 05, 0.7, 0.9)$ results in augmentation of the scattered intensity. When the BPLSB interacts with a metamaterial PEMC sphere, the intensity distribution is greatly affected by

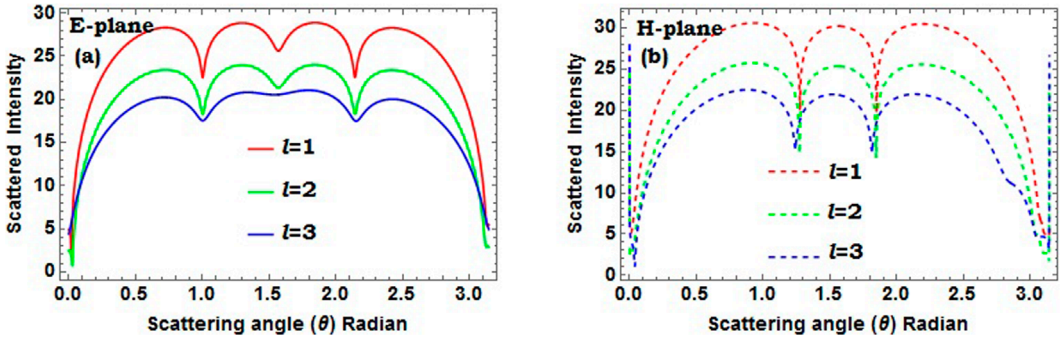

FIGURE 5
Far-field scattered intensity for PEMC sphere for various beam order (l) with $\rho = 2$, $\alpha_0 = 0.1$, and $M = 5$ **(a)** E-plane **(b)** H-plane.

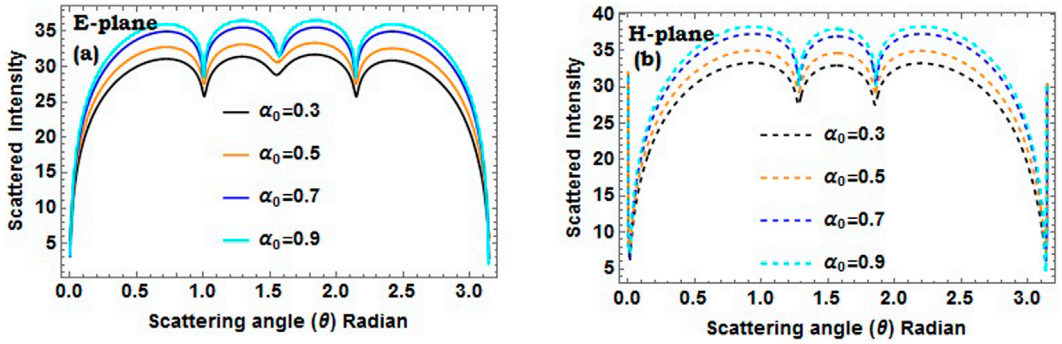

FIGURE 6
Far-field scattered intensity for PEMC sphere for various real beam scaling parameter (α_0) with $l = 1$, $\rho = 2$, and $M = 5$ **(a)** E-plane **(b)** H-plane.

varying α_0. When α_0 augments, the beam becomes more focused. It means that the beam's area gets narrower. Because of this, the intensity distribution of the metamaterial PEMC sphere gets higher in the middle of the beam. More of the scattering lobes appear for the scattering angle $\approx (1.0 - 2.0)\,rad$ for both scattering planes, i.e., E and H.

Figure 7 shows the effect of scalar admittance (M) on the BPLSB scattering efficiency (Q_{sca}) for the PEMC sphere. The electromagnetic admittance (M) is crucial to understand the optical characteristics. Increasing M for four values, such as $2, 3, 5$, and 10 results in decreasing the scattering efficiency (Q_{sca}). On varying the PEMC admittance M, the beam profile changes, and consequently the scattering efficiency factor varies as well. Categorically, the increase of M decreases the scattering rate, with an analogous behavior regarding the variation in magnitude of the scattering oscillations concerning scattering efficiency. For the dimensionless sphere size parameter, $\rho \approx 0 - 3$, the scattering efficiency increases up to its maximum, while for $\rho \approx 3 - 6$, Q_{sca} decays. However, from $\rho \approx 6$ onwards, a decreasing oscillating pattern can be observed for scattering efficiency.

Figure 8 shows the behavior of the scattering efficiency of BPLSB for varying the real scaling parameter. The scaling parameter is varied as $\alpha_0 = 0.05, 0.10$, and 0.20, respectively. The scaling parameter greatly influences how nonlinear effects change the scattering efficiency of a BPLSB because of its interaction with the metamaterial PEMC sphere. The beam scaling parameter influences the primary intensity profile as the BPLSB propagates. The scattering efficiency is enhanced owing to optical effects caused by increasing α_0 with the PEMC spherical surface. Now, increasing $\rho \approx 2 - 7$, the amplitude for scattering efficiency increases up to its maximum and then decays. For $\rho \approx 8 - 15$, the cycle repeats but with smaller amplitude. The interference between incident and scattered waves become significant. The outcome is a forward scattering response and the appearance of more obvious oscillations or ripples. The BPLSB's energy is concentrated into a smaller area as α_0 increases, leading to a more focused beam. This improves contact with the spherical surface of the PEMC scatterer by generating more intense field gradients at the location of the focus point.

Figure 9 exhibits the impact of beam order (l) on the beam scattering efficiency (Q_{sca}). The beam order (l) is crucial in BPLSB for influencing the intensity profile. For $(l = 0)$, the initial beam shape of the intensity profile of the BPLSB is that of a fundamental Bessel beam. For a PEMC sphere, which implements mixed BCs, i.e., combining both incident and scattered electromagnetic fields, the optical scattering depends on the interaction of the incident fields with the spherical surface of the PEMC. Because of the improved interaction between the structured BPLSB and the BCs of the PEMC scatterer, the scattering efficiency is decreased. So, the scattering efficiency represses as l augments because the metamaterial PEMC sphere links with the structured beam field of the BPLSB with

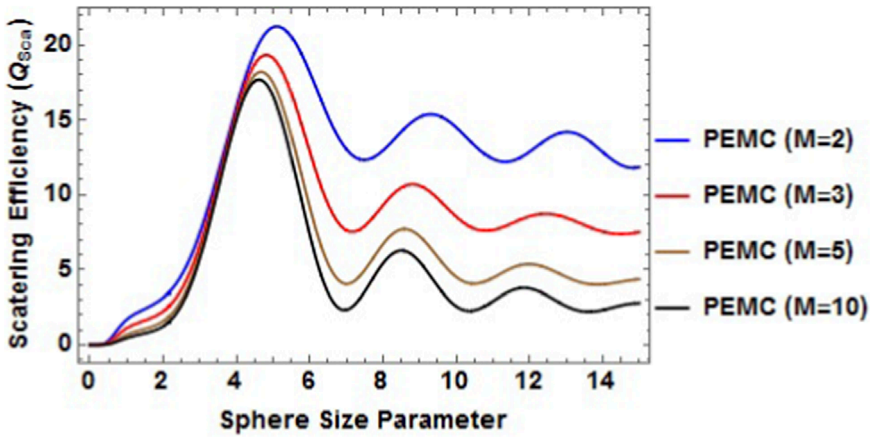

FIGURE 7
Scattering efficiency for PEMC sphere for various electromagnetic scalar admittance parameter (M) with $l = 1$ and $\alpha_0 = 0.1$.

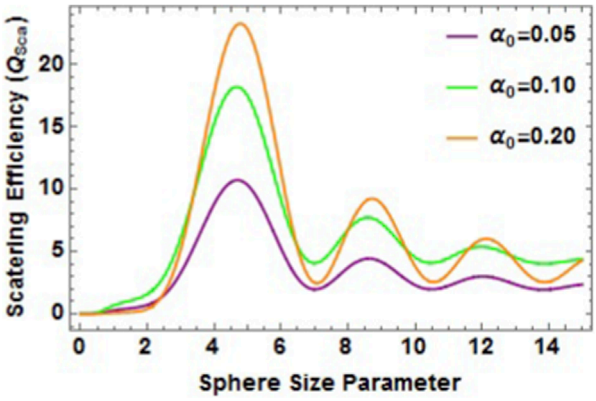

FIGURE 8
Scattering efficiency for PEMC sphere for various real scaling parameter (α_0) with $l = 1$ and $M = 5$.

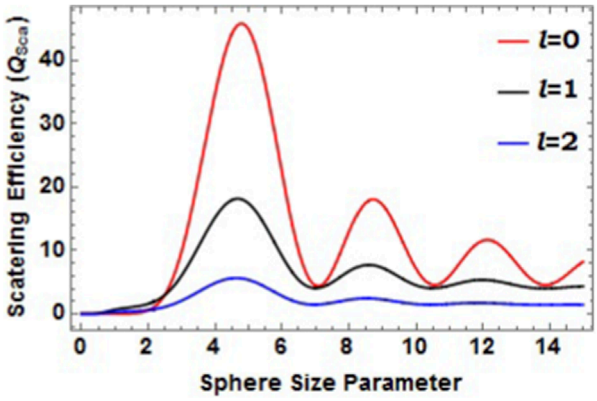

FIGURE 9
Scattering efficiency for PEMC sphere for various order of the beam (l) with $\alpha_0 = 0.1$ and $M = 5$.

smaller beam field gradients at the optical center of the BPLSB. In particular, for multipoles of low order, this weakens the coupling with the spherical scatterer of the PEMC, which in turn decreases the scattering efficiency (Q_{sca}) and electromagnetic field interaction.

This work is excellent for discussing the following: scatterers in spherical forms, linear optics, arbitrary BPLSBs order, and far-field factors. It has well-organized analytical theory, ordered computation, and clear description of all the possible configuration parameters of BPLSB as well as the PEMC scatterer. Some limitations are associated with it, including the condition for perfect sphericity, the omission of nonlinear effects, accurate metamaterial models, and precise beam parameter settings.

4 Conclusions

In this work, the scattering of the BPLSB with a metamaterial PEMC sphere, on the basis of the GLMT, has been investigated. The scattering intensity and scattering efficiency of the PEMC scatterer can be controlled by varying the BPLSB constitutive parameters, such as beam order $\boldsymbol{l}$, beam scaling parameter $\boldsymbol{\alpha_0}$, PEMC admittance $\boldsymbol{M}$, and dimensionless size parameter of the metamaterial PEMC sphere $\boldsymbol{\rho}$. The characteristic amplitude of BPLSB is observed to decay with increasing size parameter. The beam order, or the beam constant, i.e., $\boldsymbol{\alpha_0}$, governs the interference phenomena between the electromagnetic fields. By changing the values of the electromagnetic admittance, the optical characteristics in the context of FSI and scattering efficiency can be tuned very well. The characteristic pattern of scattering dynamics for BPLSB is established to be more complex when compared with a plane wave. The variation in beam configuration parameters $(\boldsymbol{l}\,\&\,\boldsymbol{\alpha_0})$ imparts unique characteristics to electromagnetic scattered field intensity and scattering efficiency. This work is valuable to provide further theoretical insights into the interaction between BPLSBs and classes of metamaterials. This work is advantageous for various domains, such as optical trapping and

sorting, optical guiding, particle characterization and dynamics, and manipulation.

Data availability statement

The original contributions offered in the work are included in the manuscript, and further details on the data from the research are provided within the article.

Author contributions

MA: Writing – original draft, Methodology, Formal Analysis, Investigation, Software, Writing – review and editing. HA: Writing – review and editing, Funding acquisition, Investigation. MH: Funding acquisition, Writing – review and editing. SA: Funding acquisition, Formal Analysis, Investigation, Writing – review and editing. AA: Writing – review and editing, Validation, Formal Analysis, Funding acquisition.

Funding

The authors declare that financial support was received for the research and/or publication of this article. This research was funded by Taif University, Saudi Arabia, project No (TU-DSPP-2024-87).

Acknowledgements

H. M. Alkhoori acknowledges the United Arab Emirates University for financially supporting this work under grant number G00004941. Also, the authors extend their appreciation to Taif University, Saudi Arabia, for supporting this work through project number (TU-DSPP-2024-87).

Conflict of interest

The authors declare that the research was conducted in the absence of any commercial or financial relationships that could be construed as a potential conflict of interest.

Generative AI statement

The authors declare that Generative AI was used in the creation of this manuscript. During the preparation of this work, the authors used ChatGPT for formatting and styling purposes. The authors take full responsibility for the content of the publication.

Any alternative text (alt text) provided alongside figures in this article has been generated by Frontiers with the support of artificial intelligence and reasonable efforts have been made to ensure accuracy, including review by the authors wherever possible. If you identify any issues, please contact us.

Publisher's note

References

1. Borja AL. *Metamaterials: devices and applications*. Norderstedt: BoD–Books on Demand (2017).

2. Sihvola A. Metamaterials in electromagnetics. *Metamaterials* (2007) 1(1):2–11. doi:10.1016/j.metmat.2007.02.003

3. Capolino F. *Theory and phenomena of metamaterials*. Boca Raton: CRC Press (2017).

4. Capolino F. *Applications of metamaterials*. Boca Raton: CRC Press (2017).

5. Lindell I, Sihvola A. Perfect electromagnetic conductor (PEMC) in electromagnetics. In: *Electromagnetics research Symposium (PIERS 2005)*. Hangzhou, China (2005).

6. Arfan M, Ghaffar A, Alkanhal MAS, Khan Y, Alqahtani AH, Shakir I. Extinction efficiency and scattering asymmetry of a PEMC sphere illuminated by vortex electromagnetic waves. *Opt Quan Electronics* (2023) 55(10):891. doi:10.1007/s11082-023-05156-2

7. Sihvola A, Lindell IV. Possible applications of perfect electromagnetic conductor (PEMC) media. In: *2006 first European conference on antennas and propagation*. IEEE (2006).

8. Tang H, Li R, Gong S, Wei B, Yang L, Zhu Z, et al. Scattering of arbitrary-shaped optical polarized beams by a PEMC sphere. *J Quantitative Spectrosc Radiative Transfer* (2022) 281:108101. doi:10.1016/j.jqsrt.2022.108101

9. Lindell IV, Sihvola A. Reflection and transmission of waves at the interface of perfect electromagnetic conductor (PEMC). *Prog In Electromagnetics Res B* (2008) 5:169–83. doi:10.2528/pierb08022010

10. Zahra T, Salam A, Jafri A, Naqvi Q. Study of polarizabilities for a PEMC sphere in chiral metamaterial. *Optik* (2016) 127(4):1827–32. doi:10.1016/j.ijleo.2015.10.180

11. Tang H, Wei B, Li R, Yang L, Gong S, Yang R, et al. Radiation force and torque caused by the interaction between arbitrary-shaped optical polarized beams and a PEMC sphere. *J Quantitative Spectrosc Radiative Transfer* (2022) 296:108436. doi:10.1016/j.jqsrt.2022.108436

12. Ghaffar A, Alkanhal MA. High frequency scattering of a Gaussian beam by a perfect electromagnetic conductor (PEMC) cylinder. *Optik* (2016) 127(7):3680–3. doi:10.1016/j.ijleo.2015.12.130

13. Durnin J, Miceli J, Jr, Eberly JH. Diffraction-free beams. *Phys Rev Lett* (1987) 58(15):1499–501. doi:10.1103/physrevlett.58.1499

14. Chávez-Cerda S. A new approach to Bessel beams. *J Mod Opt* (1999) 46(6):923–30. doi:10.1080/09500349908231313

15. Zhang S, Chen S, Wei Q, Li R, Wei B, Song N. Scattering of a bessel pincer light-sheet beam on a charged particle at arbitrary size. *Micromachines* (2024) 15(8):975. doi:10.3390/mi15080975

16. Mitri F. Interaction of bessel pincers light-sheets with an absorptive subwavelength sphere coated by a plasmonic layer. *J Opt Soc America B* (2017) 34(7):1471–7. doi:10.1364/josab.34.001471

17. Zhang S, Li R, Wei B, Song N, Yang L, Sun H. Scattering of a non-paraxial bessel pincer light-sheet by a dielectric sphere of arbitrary size. *J Quantitative Spectrosc Radiative Transfer* (2021) 268:107647. doi:10.1016/j.jqsrt.2021.107647

18. Zhang S, Li R, Wei B, Zhang J, Sun H, Song N. Scattering of a non-paraxial bessel light-sheet by a sphere of arbitrary size. *J Quantitative Spectrosc Radiative Transfer* (2020) 245:106869. doi:10.1016/j.jqsrt.2020.106869

19. Zhang S, Wei B, Wei Q, Li R, Song N, Radiation force of bessel pincer light-sheets on a nanoscale dielectric sphere. In: *Mesophotonics: Physics and systems at mesoscale*. SPIE (2022).

20. Gréhan G. Evaluation of a particle sizing technique based on laser sheets. *Part and Part Syst characterization* (1994) 11(1):101–6. doi:10.1002/ppsc.19940110113

21. Pei S, Pan Q, Cui F, Xu S, Cao Z. Electromagnetic scattering of an airy beam light sheet by a multilayered sphere. *Optik* (2019) 180:379–86. doi:10.1016/j.ijleo.2018.11.130

22. Arfan M. Electromagnetic scattering by a homogenous spherical particle using non-diffracting focused airy beam. *Phys Wave Phenomena* (2025) 33(4):327–35. doi:10.3103/S1541308X25600205

23. Laskin A, Laskin V. Beam shaping to generate uniform laser light sheet and linear laser spots. In: *Laser beam shaping XIV*. SPIE (2013).

24. Mitri F. Radiation force and torque of light-sheets. *J Opt* (2017) 19(6):065403. doi:10.1088/2040-8986/aa6c73

25. Vettenburg T, Dalgarno HIC, Nylk J, Coll-Lladó C, Ferrier DEK, Čižmár T, et al. Light-sheet microscopy using an airy beam. *Nat Methods* (2014) 11(5):541–4. doi:10.1038/nmeth.2922

26. Zhao M, Zhang H, Li Y, Ashok A, Liang R, Zhou W, et al. Cellular imaging of deep organ using two-photon bessel light-sheet nonlinear structured illumination microscopy. *Biomed Opt Express* (2014) 5(5):1296–308. doi:10.1364/boe.5.001296

27. Yin J, Liang R, Hou H, Miao Y, Yu L. Light sheet fluorescence microscopy with active optical manipulation. *Opt Lett* (2024) 49(5):1193–6. doi:10.1364/ol.515280

28. Zhang S, Wei B, Wei Q, Li R, Chen S, Song N. Optical force of bessel pincer light-sheets beam on a dielectric sphere of arbitrary size. *Nanomaterials* (2022) 12(21):3723. doi:10.3390/nano12213723

29. Mitri F. Nonparaxial bessel and bessel–gauss pincers light-sheets. *Phys Lett A* (2017) 381(3):171–5. doi:10.1016/j.physleta.2016.10.055

30. Arfan M, Khaleel N, Ghaffar A, Khan Y, Shakir I. Study of scattering for a PEMC sphere with bessel beam illumination. *Opt Quan Electronics* (2023) 55(5):443. doi:10.1007/s11082-023-04701-3

31. Arfan M, Asif M, Ghaffar A, Razzaz F, Saeed S, Alanazi T. Analysis of scattering characteristics of PEMC sphere by vortex bessel beams. *Optik* (2024) 298:171599. doi:10.1016/j.ijleo.2023.171599

32. Tang H, Shi Z, Zhang Y, Li R, Wei B, Gong S, et al. Scattering of a radially polarized bessel beam by a PEMC sphere: photonic nanojet and bottle beam formation. *Appl Opt* (2023) 62(34):9164–74. doi:10.1364/ao.506734

33. Asif M, Arfan M, Althobaiti S, Althobaiti A, Zhang Y, Li R, et al. Scattering characteristics of non-diffracting lommel beam by a metamaterial PEMC sphere. *Opt Quan Electronics* (2024) 56(7):1242. doi:10.1007/s11082-024-07178-w

34. Shi Y, Song X. Sequential immunotherapy for alopecia areata: phase-driven immune rebalancing. *Rn* (2025) 2(1):1–14. doi:10.1080/1744666X.2025.2585344

35. Arfan M. Radar cross section (RCS) of perfect electromagnetic conductor (PEMC) cylinder by a laguerre–gaussian beam. *Kuwait J Sci* (2021) 1–10. doi:10.48129/kjs.19021

36. Arfan M. *Electromagnetic radiation force of vortex electromagnetic wave exerted on a perfect electromagnetic conductor (PEMC) sphere: 10.48129/kjs. 20775*. Amsterdam: Elsevier B.V. (2021).

37. Gouesbet G, Gréhan G *Generalized lorenz-mie theories*, 31. Springer (2011).

38. Lock JA, Gouesbet G. Generalized lorenz–mie theory and applications. *J Quantitative Spectrosc Radiative Transfer* (2009) 110(11):800–7. doi:10.1016/j.jqsrt.2008.11.013

39. Ruppin R. Scattering of electromagnetic radiation by a perfect electromagnetic conductor sphere. *J Electromagn Waves Appl* (2006) 20(12):1569–76. doi:10.1163/156939306779292390